Journal of Solid State Chemistry 183 (2010) 2779–2785

Contents lists available at ScienceDirect

Journal of Solid State Chemistry

journal homepage: www.elsevier.com/locate/jssc

Solvothermal synthesis and luminescence properties of monodisperse Gd_2O_3:Eu^{3+} and Gd_2O_3:Eu^{3+}@SiO_2 nanospheres

Yu Wang, Xue Bai, Tong Liu, Biao Dong, Lin Xu, Qiong Liu, Hongwei Song *

State Key Laboratory on Integrated Optoelectronics, College of Electronic Science and Engineering, Jilin University, 2699 Qianjin Street, Changchun 130012, People's Republic of China

ARTICLE INFO

Article history:
Received 17 May 2010
Received in revised form
26 August 2010
Accepted 1 September 2010
Available online 8 September 2010

Keywords:
Solvothermal synthesis
Gadolinium oxide
Europium
Luminescence
core–shell structure

ABSTRACT

A series of uniform, monodispersed $Gd(OH)^3$:Eu^{3+} nanospheres less than 100 nm were successfully synthesized with iron ions as catalyst and DMF as solvent under the solvothermal condition. Cetyltrimethyl ammonium bromide (CTAB) and Polyvinylpyrrolidone (PVP) were performed as co-surfactant during this facile procedure should be changed as A series of uniform, monodisperse $Gd(OH)^3$:Eu^{3+} nanospheres less than 100 nm in diameter were successfully synthesized with solvothermal method. Iron ion was used as catalyst and Dimethylformamide (DMF) as solvent, Cetyltrimethyl Ammonium Bromide (CTAB) and Polyvinylpyrrolidone (PVP) were performed as surfactants. Further calcination process was applied to prepare Gd_2O_3:Eu^{3+} nanoshpheres during this facile procedure.

1. Introduction

Nanomaterials have continuously attracted worldwide interest because the morphology, dimensionality, and size of the materials have great effects on their physical and chemical properties [1–6]. The varieties of morphologies, monodisperse zero-dimensional nanospheres have been widely studied due to their potential applications in medical diagnostic and therapeutic fields [7,8]. Recently, a number of synthesis methods have been employed in preparation of nanomaterials, for example, thermal pyrolysis, coprecipitation technique, hydrothermal or solvothermal method, and so on. Among these synthesis methods, hydro-/solvothermal methods have been widely used to prepare a number of nano-/microcrystals [9–13].

Rare earth (RE) nanomaterials are the most promising materials for a variety of applications in high performance luminescent devices, lighting, displays, and biolabels [14–20]. Over the past decade, a variety of RE one-dimensional and two-dimensional RE nano-/microstructures, such as rods, wires, tubes, belts and plates, have been synthesized through hydro-/solvothermal process [21–26]. Compared with the former reports, there are less reports on the synthesis of uniform monodisperse nanospherical RE nanomaterials through solvothermal method [27–29]. As is well known, Eu^{3+}-doped Gd_2O_3 nanospherical phosphor is one of the important fluorescent markers in a variety of immunosensing applications. Moreover, the compound containing Gd^{3+} is a known contrast agent for magnetic resonance imaging (MRI). Monodispersed RE doped Gd_2O_3 nanospheres with size less than 100 nm is very required to function as both fluorescence and MRI labels in biomedical field [30,31]. For bio-applications, water solubility of the nanocrystals (NCs) is also crucial; numerous efforts have been made to transfer the NCs from hydrophobic to hydrophilic. The most popular strategy was surface hydroxylation. Some works have been performed to coat RE oxide nanophosphors with SiO_2 shells, which contain a number of –OH bonds on the surface of the nanoparticles and can link with biomaterials. Unfortunately, all the results on coating RE oxide nanophosphors seemed to be unideal, because the RE oxide nanoparticles being coated were not uniform and monodisperse [32]. Therefore, synthesis of monodispersed Eu^{3+} doped Gd_2O_3 nanosphere with size less than 100 nm and relative Gd_2O_3:Eu^{3+}@SiO_2 core–shell nanosphere and understanding of their spectroscopic properties are significant for biomedical application.

In this work, we present the syntheses of uniform and monodisperse Eu^{3+} doped $Gd(OH)_3$ and Gd_2O_3 nanospheres by a DMF solvothermal method with the assistance of iron ion, CTAB and PVP and the preparation of the ideal Gd_2O_3:Eu^{3+}@SiO_2 core–shell nanocomposites by the modified Stöber method. The luminescent properties of Gd_2O_3: Eu^{3+} and Gd_2O_3:Eu^{3+}@SiO_2 samples such as emission intensity and lifetime are systemically studied.

* Corresponding author. Fax: +86 431 85155129.
E-mail address: hwsong2005@yahoo.com.cn (H. Song).

0022-4596/$ - see front matter © 2010 Elsevier Inc. All rights reserved.
doi:10.1016/j.jssc.2010.09.002

2. Experimental section

2.1. Materials

All reagents were used without further purification. Gadolinium nitrate ($Gd(NO_3)_3 \cdot 5H_2O$), Iron chloride ($FeCl_3 \cdot 6H_2O$) and Europium nitrate ($Eu(NO_3)_3 \cdot 5H_2O$) were purchased as inorganic source. CTAB and PVP (K30) were purchased as co-surfactant. The DMF was used as solvent. The TEOS was selected as silicon source.

2.2. Synthesis

A series of $Gd(OH)_3:Eu^{3+}$ nanospheres were prepared through the solvothermal method. In the synthesis, 0.20 g gadolinium nitrate ($Gd(NO_3)_3 \cdot 5H_2O$), 0.01 g europium nitrate ($Eu(NO_3)_3 \cdot 5H_2O$) and different amounts of ($FeCl_3 \cdot 6H_2O$) were first dissolved in DMF(10 mL), and then amounts of CTAB were added with stirring, together with amounts of PVP, to form a yellow suspension. The resulting suspension was stirred for 12 h until it was homogenous, and then sealed in a Teflon-lined stainless steel autoclave. All of the above-mentioned manipulations were performed in ambient atmosphere. The autoclaves were heated at 180 °C for 24 h under static condition and then allowed to cool in ambient atmosphere. The light brown powders were centrifugated and washed three times with ethanol, then air-dried at 60 °C.

Thermal conversion of $Gd(OH)_3$ to Gd_2O_3. The as prepared $Gd(OH)_3$samples were annealed at 550 °C for 4 h in air to obtain the Gd_2O_3 products. In order to investigate the luminescence of Eu^{3+} in the host Gd_2O_3 nanospheres, the Eu^{3+}-doped Gd_2O_3 samples were prepared by introducing proper amounts of $Eu(NO_3)_3 \cdot 5H_2O$ into the yellow suspension.

Silica coating on $Gd_2O_3:Eu^{3+}$ nanosphere. Silica coated $Gd_2O_3:Eu^{3+}$ were prepared via the modified Stőber method. Typically, 50 mg of $Gd(OH)_3:Eu^{3+}$ nanospheres precursor was ultrasonically dispersed in a solution containing 80 mL of ethanol and 10 mL of distilled water for 30 min to give rise to a suspension. Under vigorous stirring, 0.15 g CTAB was added into the mixed solution, followed by the addition of ammonia (0.2 mL, 28 wt%), then TEOS (0.064 mL) was added into the mixed solution. After being stirred for 24 h, the reaction mixture was centrifuged and then redispersed into ethanol for further washing. The products were washed with absolute ethanol three times, then air-dried at 60 °C. Finally, the as silica coated $Gd(OH)_3:Eu^{3+}$ samples were annealed at 550 °C for 4 h in air to obtain the $Gd_2O_3:Eu^{3+}@SiO_2$ core–shell nanospherical product.

2.3. Characterization

The crystal structures of the $Gd_2O_3:Eu^{3+}$ products were inspected with a Rigaku D/max 2550 X-ray diffractometer, using a monochromatized Cu target radiation resource ($\lambda = 1.54$ Å). The surface morphology of the $Gd(OH)_3:Eu^{3+}$ nanospheres and $Gd_2O_3:Eu^{3+}$ nanospheres were performed with a JEOL JSM-7500 field emission scanning electron microscope at an accelerating voltage of 15 kV. The transmission electron micrograph (TEM) images were recorded on a JEM-2010 transmission electron microscope under a working voltage of 200 kV. The high resolution transmission electron micrograph (HRTEM) images and selected area electron diffraction (SAED) pattern were recorded on a JEM-2010F high resolution transmission electron microscope under a working voltage of 200 kV. The X-ray photoelectron spectra (XPS) were measured by ESCAlab 250 Analytical XPS spectrometer. The excitation and emission spectra were recorded on a JPL Sens-9000 fluorescence spectrometer. Fluorescence dynamics were investigated by a laser system consisting of an Nd:YAG pump source and a tunable OPO laser (Continuum Precision II 8000).

3. Results and discussion

3.1. Morphology and structural characterization of $Gd(OH)_3:Eu^{3+}$, $Gd_2O_3:Eu^{3+}$ and $Gd_2O_3:Eu^{3+}@SiO_2$

First of all, the $Gd(OH)_3:Eu^{3+}$ nanospheres with the molar ratio of iron chloride to gadolinium nitrate were 0.025, 0.075, 0.1 and 0.3 in the starting materials, and are named GNP-1, GNP-2, GNP-3 and GNP-4, respectively. The morphologies of these $Gd(OH)_3:Eu^{3+}$ products were characterized by SEM. As shown in Fig. 1, the samples GNP-1, GNP-2 and GNP-3 present uniform nanospheres with diameters from 80 to 100 nm. But the morphology of the sample GNP-4 is not as uniform as those of the morphology of the samples GNP-1, GNP-2 and GNP-3, even though only the iron content in the starting materials was changed but the other conditions kept constant in the whole process. Furthermore, it also can be observed that the surfaces of all GNP-1 to GNP-4 samples are coarse, which indicates that these nanospheres consist of very small nanocrystallines. Fig. 2 shows the relative SEM images of $Gd_2O_3:Eu^{3+}$ products annealed at the relative parent's $Gd(OH)_3:Eu^{3+}$ at 550 °C for 4 h, named as GNP-1a, GNP-2a, GNP-3a and GNP-4a, respectively. It can be found that the calcined GNP-1a, GNP-2a and GNP-3a products with size from 70 to 90 nm are also composed of uniform nanospheres, which are similar to their corresponding parent $Gd(OH)_3:Eu^{3+}$ nanospheres. The SEM image shown in Fig. 2d reveals that the morphology of GNP-4a becomes more irregular after being annealed compared with the morphologies of GNP-1a, GNP-2a and GNP-3a. It can be seen that the $Gd_2O_3:Eu^{3+}$ nanospheres, inheriting their parent's morphologies, have a monodisperse property, with no evident aggregation through the calcination process. Fig. 3 shows the TEM images of the $Gd_2O_3:Eu^{3+}$ nanospheres and HRTEM images and SAED pattern of $Gd_2O_3:Eu^{3+}@SiO_2$ core–shell composites. Fig. 3a further shows that the $Gd_2O_3:Eu^{3+}$ nanospheres are uniform and monodisperse. Fig. 3b, c, and d presents the images of $Gd_2O_3:Eu^{3+}$ coated with a silica layer. It can be clearly observed that the particles have a core–shell structure and the silica shell is clearly visible. The thickness of the silica shells is uniform (15 nm). The inset SAED pattern in Fig. 3c reveals the polycrystalline nature of the sample. It also indicates that the $Gd_2O_3:Eu^{3+}$ nanospheres consist of a number of small nanocrystals with size of about 5 nm, which is in agreement with the magnified selected section of single $Gd_2O_3:Eu^{3+}$ nanosphere as seen in Fig. 3d. HRTEM image (Fig. 3d) of different nanocrystals provided more detailed information about the local structure. The lattice planes continuously extending in each nanocrystal showed good crystallinity of the nanocrystal. The distance of the lattice planes extending on the same direction in each nanocrystal was calculated to be 0.32 and 0.20 nm, respectively, which could be assigned to the (2 2 2) and (4 4 0) planes of cubic phase Gd_2O_3, respectively. It should be highlighted that the resulting silica surface of $Gd_2O_3:Eu^{3+}@SiO_2$ nanocomposites is very important for straightforward surface functionalization with different functional groups, for example, amino or carboxyl groups via silica surface chemistry. Moreover, the functionalized nanocomposite can be used for further covalent conjugation with different biomolecules.

The XRD patterns of the GNP-1a to GNP-4a nanospheres are shown in Fig. 4. For comparison, the peak positions of all the samples exactly match that of cubic phase of Gd_2O_3 (JCPDS No. 86-2477), even though all the samples contain Eu^{3+} ions. No other impurity peaks can be detected, indicating that the Eu^{3+} ions have

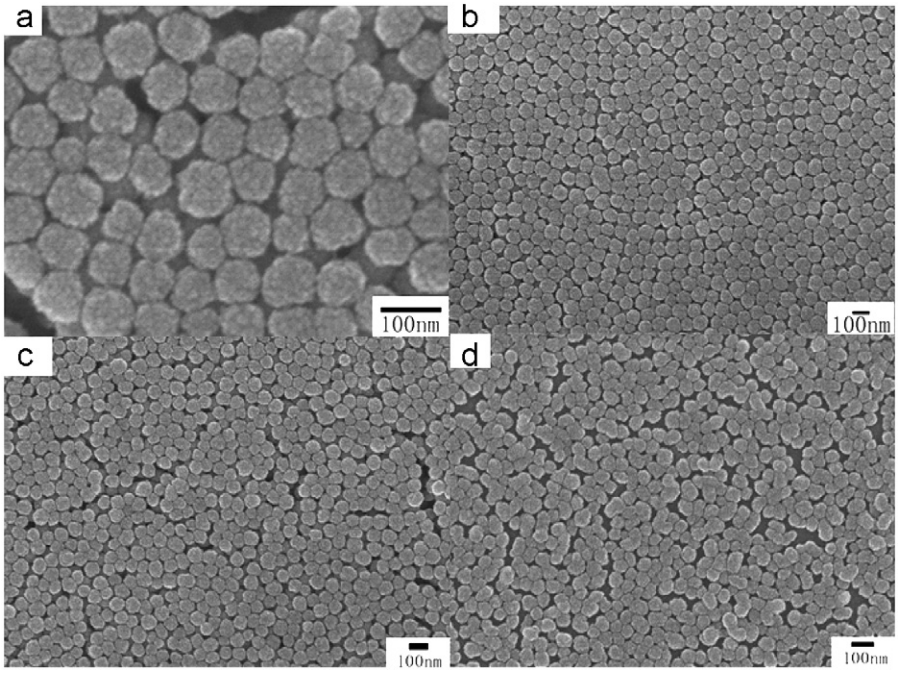

Fig. 1. SEM images of $Gd(OH)_3:Eu^{3+}$ samples: (a) GNP-1, (b) GNP-2, (c) GNP-3 and (d) GNP-4.

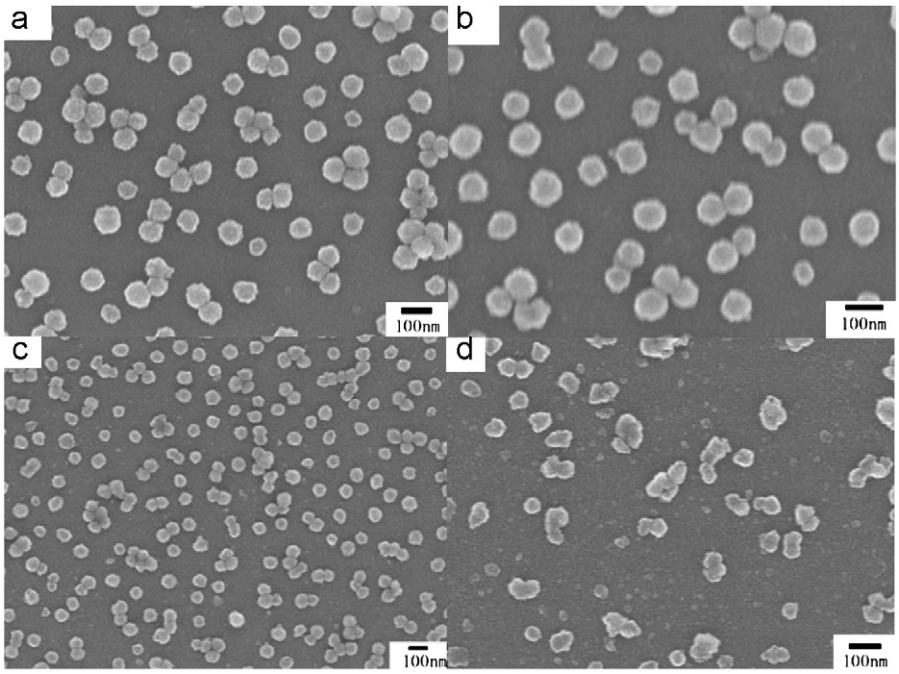

Fig. 2. SEM images of $Gd_2O_3:Eu^{3+}$ samples: (a) GNP-1a, (b) GNP-2a, (c) GNP-3a and (d) GNP-4a.

been thoroughly doped into the Gd_2O_3 host lattice. In addition, due to the radius of the iron ion (64 pm) being quite different from that of Gd ion (94 pm), the peak positions of XRD pattern will shift if the iron elements are doped into the Gd_2O_3 lattices. However, the peak positions of these $Gd_2O_3:Eu^{3+}$ do not shift, which suggests there is no iron ion doped into the Gd_2O_3 nanospheres. It should be noted that the intensity of GNP-4a obviously decreases in comparison with the other three samples, indicating that the high content of iron ion in the starting material can decrease the crystallinity of the final product in the synthetic process.

High resolution X-ray photoelectron spectra (XPS) were measured to characterize the surface electronic structure and chemical element valence by referencing the C1s line to 284.5 eV, as shown in Fig. 5. The survey XPS spectra reveal that all the products contain Gd, O elements. No distinct peaks at bonding energies of 708.2 eV for Fe $2P_{3/2}$ and 722.3 eV for Fe $2P_{1/2}$ were distinguished, indicating the inexistence of iron element in the final products, although a different amount of iron chloride was added into the starting materials. This result is well in agreement with the powder XRD patterns.

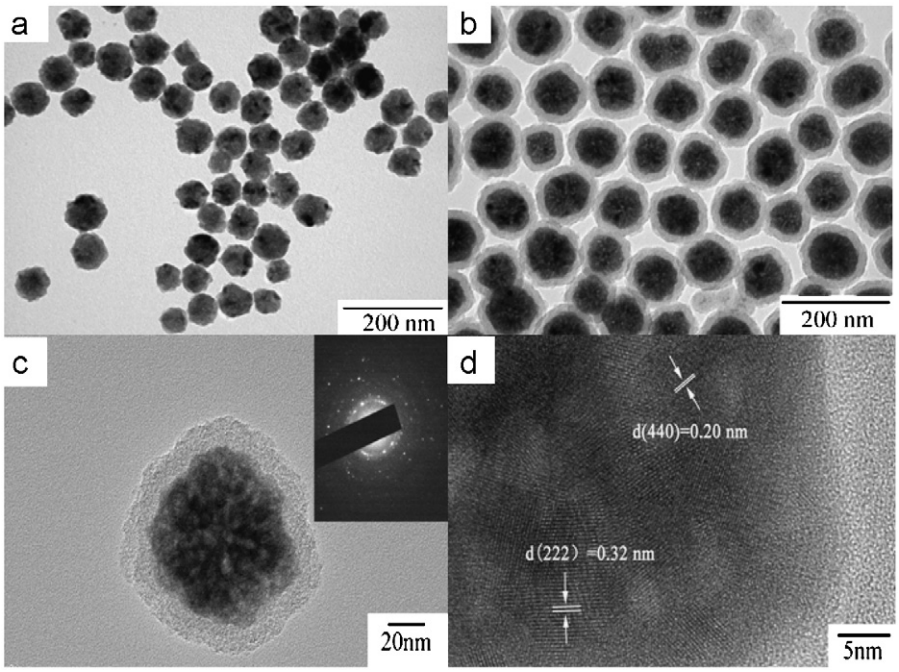

Fig. 3. TEM image of Gd_2O_3:Eu^{3+} sample: (a) GNP-1a; and HRTEM images and SAED pattern of Gd_2O_3:Eu^{3+}@SiO_2 sample: (b)Gd_2O_3:Eu^{3+}@SiO_2, (c) single nanosphere and SAED of Gd_2O_3:Eu^{3+}@SiO_2, and (d) magnified single nanosphere of Gd_2O_3:Eu^{3+}@SiO_2.

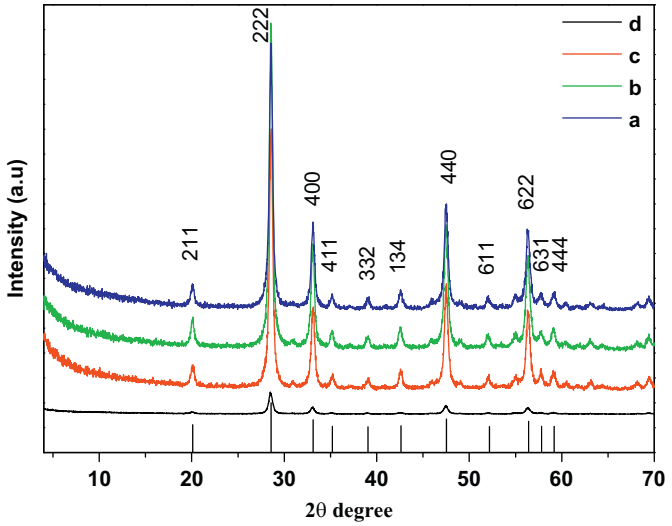

Fig. 4. The X-ray powder diffraction patterns of Gd_2O_3:Eu^{3+} samples: (a) GNP-1a, (b) GNP-2a, (c) GNP-3a and (d) GNP-4a.

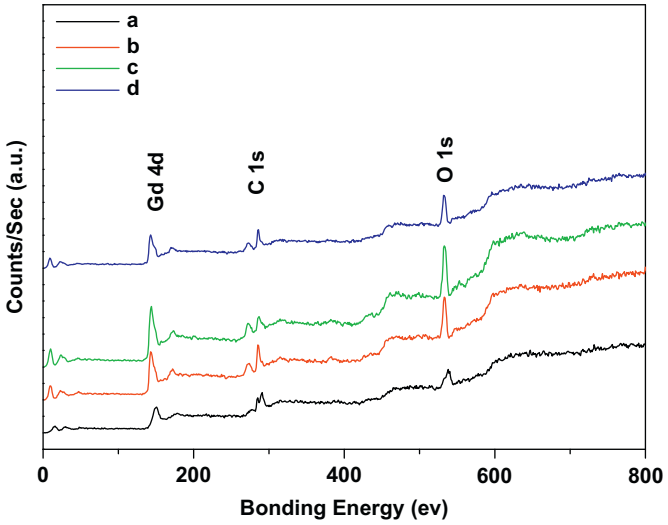

Fig. 5. The survey XPS spectrum of as-obtained samples: (a) GNP-1a, (b) GNP-2a, (c) GNP-3a and (d) GNP-4a.

3.2. *Formation mechanism for $Gd(OH)_3$:Eu^{3+} nanosphere*

In the solvothermal synthesis process, two kinds of surfactants (CTAB and PVP) and iron chloride were used. In order to know the influence of experimental parameters on the effect of the morphologies of gadolinium hydroxide, a series of control experiments were performed. As revealed by Fig. S1, there is an irregular bulk product to be obtained when the CTAB and PVP were absent in the reaction system; Fig. S2 shows that the irregular product was formed even though the CTAB was present while PVP was absent in the starting materials. In addition, no solid product was obtained when only PVP was added into the starting materials without CTAB in the starting materials. In Fig. S3, there was a few uniform nanospheres to be synthesized when CTAB and PVP coexisted in the starting materials without iron chloride in the starting materials. At last, the uniform and monodisperse nanosphere was obtained when the amount of iron chloride was in the molar ratio range from 0.025 to 0.1 with the CTAB and PVP in the reaction system. However, when the molar ratio of iron chloride was over 0.1 with other conditions keeping unchanged, the morphology of the product became irregular (Supporting Information, Fig. S4).

It is believed that the amount of CTAB may undergo a dissolving process to produce positive ionic species such as CTA^+ under solvothermal conditions, which could facilitate stabilization of the initial $Gd(OH)_3$:Eu^{3+} nucleation. Then PVP coordinates onto the Gd^{3+} ions of $Gd(OH)_3$:Eu^{3+} crystal surfaces and prevents their crystallites from rapid growth [33]. As for the shape control, in this case, the carboxyl groups of the PVP interact with CTA^+, which reduces the coordinate abilities of PVP in the

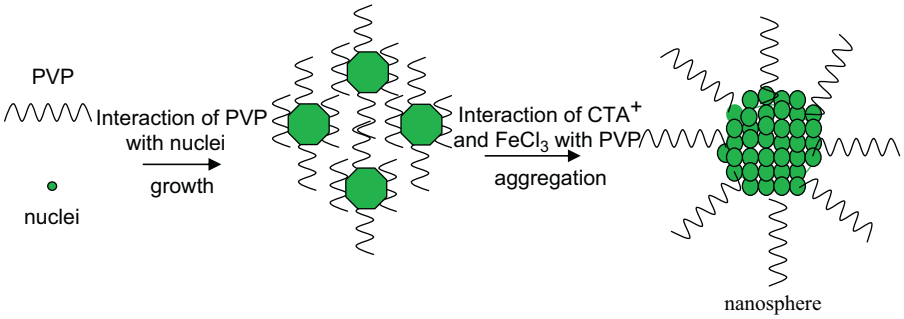

Scheme 1. Illustration of formation processes of $Gd(OH)_3:Eu^{3+}$ nanosphere.

solvothermal process. Thus PVP does not thoroughly protect the nuclei, which induces the nuclei to aggregate to give rise to forming nanospheres. The coordinate ability of PVP is further reduced because the carboxyl groups of the PVP are protonized by adding appropriate iron ion into the reaction system [34], which induces plenty of nanospheres to be obtained. On adding the molar ratio of iron chloride over 0.1 compared to gadolinium nitride, the aggregation rate of nuclei increases to produce irregular morphology with poor crystallinity. Therefore, it is possible that the iron ion may undergo hydrolysis process to produce minor proton and the proton and CTA^+ could further accelerate the self-assembly process. In order to test whether the proton could further accelerate the self-assembly process, the nitric acid, CTAB and PVP instead of iron chloride are added into the starting materials; a number of uniform and monodispersed nanospheres are also obtained (as seen in Fig. S5). Scheme 1 illustrates the formation processes of $Gd(OH)_3:Eu^{3+}$ nanosphere. This result indicates that iron chloride and acid have the same action for the morphology evolution of the gadolinium hydroxide nanomaterials. These preliminary observations seem to support the proposed roles of CTAB, PVP and iron chloride or acid in the present stage of our study.

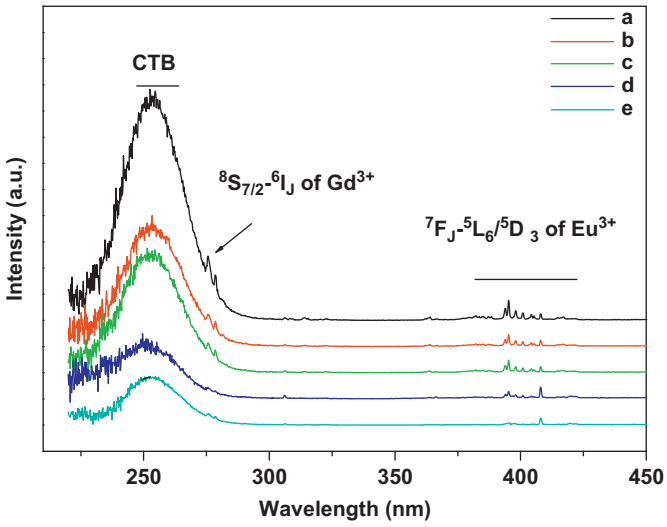

Fig. 6. Excitation spectra (λ_{em}=613 nm) of Eu^{3+} in different samples: (a) GNP-1a, (b) GNP-2a, (c) GNP-3a, (d) GNP-4a and (e) $Gd_2O_3:Eu^{3+}@SiO_2$.

3.3. *Excitation and emission spectra of $Gd_2O_3:Eu^{3+}$ and $Gd_2O_3:Eu^{3+}@SiO_2$*

Fig. 6 shows the excitation spectra of samples GNP-1a, GNP-2a, GNP-3a, GNP-4a and $Gd_2O_3:Eu^{3+}@SiO_2$. All the excitation spectra are composed of a strong and broad band in the range of 200–300 nm and a number of weak and sharp emission lines. The band is assigned to the charge-transfer (CT) transitions between O^{2-} and Eu^{3+} ions. The sharp lines around 275 nm correspond to the $^8S_{7/2}$–^6I_J transitions of Gd^{3+}, implying sufficient energy transfer (ET) from Gd^{3+} to Eu^{3+} ions. The sharp lines in the region of 350–450 nm give rise to the inner-shell *f–f* transitions of Eu^{3+} ions (^7F_J–$^5L_6$/$^5D_3$). The peak locations of the charge transfer band (CTB) in samples GNP-1a to GNP-4a are around 253, 252, 252, and 250 nm, respectively, while the location of CTB in the $Gd_2O_3:Eu^{3+}$ composites is around 252 nm. This implies that the CTB has a little shift to blue on increasing the content of iron chloride in the starting materials. It is well-known that the CTB is closely related to the covalency between O^{2-} and Eu^{3+} and the coordination environment around Eu^{3+}. In general, the Eu^{3+}, the adjacent O^{2-}, and the sub-adjacent Gd^{3+} are able to form Eu^{3+}–O^{2-}–Gd^{3+} pairs and the electrons transfer from the 2*p* orbital of O^{2-} ions to the $4f^6$ orbital of Eu^{3+} to form the CTB. The blue-shift of the CTB indicates that more energy is required to cause the electrons to migrate because the crystallinity of the host material decreases on increasing the content of iron chloride in the starting materials. It should also be noted that: (1) The emission intensity of Eu^{3+} gradually quenches with the increase of iron ions in the starting materials owing to the gradual decrease in crystallinity; (2) In comparison to the as-grown $Gd_2O_3:Eu^{3+}$, the emission intensity in the $Gd_2O_3:Eu^{3+}@SiO_2$ decreased nearly to 1/2, which was also observed in the other SiO_2 coated nanophosphors (see curves b and e) [35].

Fig. 7 shows the normalized emission spectra of different samples of $Gd_2O_3:Eu^{3+}$ and $Gd_2O_3:Eu^{3+}@SiO_2$ under the 253 nm excitation. Six groups of emission lines are observed, which are ascribed to the $^5D_1$–$^7F_1$ and $^5D_0$–^7F_J (J=0–4) transitions of the Eu^{3+} ions, as labeled in the figure. In all the emission spectra, the dominated transition is the red $^5D_0$–$^7F_2$, which is an electric-dipole allowed one and hypersensitive to the local environment. For the samples GNP-1a, GNP-2a GNP-3a and $Gd_2O_3:Eu^{3+}@SiO_2$, the emission spectra are very similar. The $^5D_0$–$^7F_2$ emission line at 613 nm is dominantly strong in contrast to the other emission lines, which is in accordance with the traditional emission spectrum of cubic $Gd_2O_3/Y_2O_3:Eu^{3+}$ [22]. For the sample GNP-4a, however, the emission spectra are quite different from those in the other samples. In contrast to the intensity of the $^5D_0$–$^7F_2$ line at 613 nm of GNP-1, GNP-2 and GNP-3 samples, the luminescent intensities of $^5D_0$–$^7F_2$ lines at 616 and 620 nm and the $^5D_0$–$^7F_4$ lines at 700 and 706 nm in GNP-4 become relatively strong. The $^5D_0$–$^7F_2$ line at 620 nm becomes the strongest peak in the emission spectrum. This can be attributed to more disordered local environments surrounding Eu^{3+} ions in the samples GNP-4a, which demonstrates poor crystallinity in contrast to the other samples. In the sample GNP-4a, the degree of noncrystallinity of

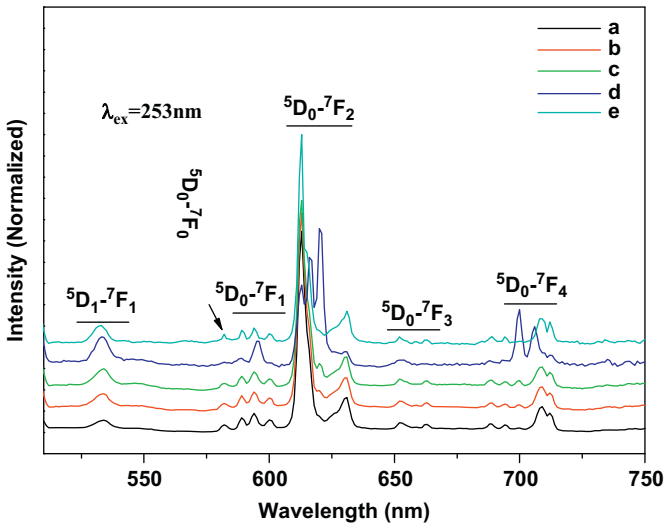

Fig. 7. Normalized emission spectra (λ_{ex}=253 nm) in different samples: (a) GNP-1a, (b) GNP-2a, (c) GNP-3a, (d) GNP-4a and (e) Gd_2O_3:Eu^{3+}@SiO_2.

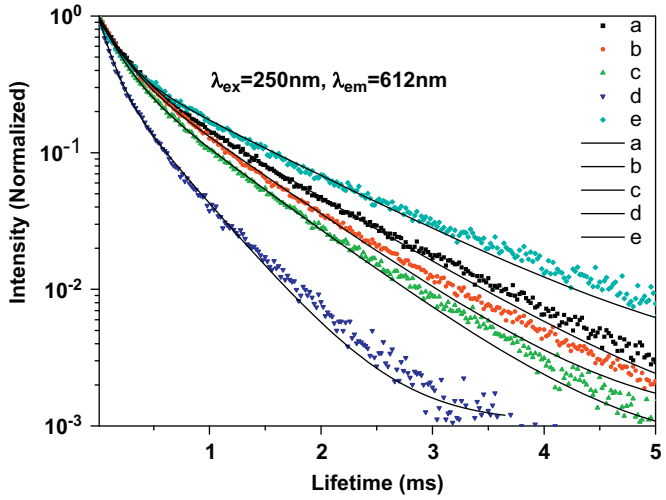

Fig. 8. Normalized luminescent decay curves of the $^5D_0$–$^7F_2$ (λ_{ex}=253 nm, λ_{em}=612 nm) transition for Eu^{3+}: (a) GNP-1a, (b) GNP-2a, (c) GNP-3a, (d) GNP-4a and (e) Gd_2O_3:Eu^{3+} @SiO_2.

Gd_2O_3:Eu^{3+} increases, and more defect states are involved in the Gd_2O_3 lattices. As a consequence, the crystal field surrounding Eu^{3+} ions degenerates, leading to a change of the emission spectrum of the $^5D_0$–^7F_J compared to the other samples, and also leading to the quenching of $^5D_0$–^7F_J overall emission intensity.

3.4. Luminescent decay dynamics

Fig. 8 shows that the luminescent decay curves for the $^5D_0$–$^7F_2$ transitions of the Eu^{3+} ions in different samples. It can be seen that all the luminescent decay curves can be well fitted by the following bi-exponential equation, which depart from exponential relationship:

$$I(t) = I_1 * \exp(-t/\tau_1) + I_2 * \exp(-t/\tau_2), \quad (1)$$

where τ_1 and τ_2 present the shorter and longer decay time constants, respectively, I_1 and I_2 present the relative contributions of the shorter and the longer components, respectively. The appearance of two decay time constants could be attributed to two kinds of local environments surrounding Eu^{3+} ions in the Gd_2O_3:Eu^{3+} nanocrystals, one is relatively ordered and the other is relatively disordered, for all the samples. The longer lifetime constants correspond to the Eu^{3+} ions surrounded by relatively ordered lattices of Gd_2O_3, while the shorter ones correspond to the Eu^{3+} ions surrounded by relatively disordered lattices. By fitting the experimental results with Eq. (1), the lifetime constants are obtained, as listed in Table 1. It can be seen that: (1) the decay time constants gradually decrease on increasing the iron concentration in the starting material on the whole, for the $^5D_0$–$^7F_2$ transitions; (2) the decay time constants in the Gd_2O_3:Eu^{3+}@SiO_2 sample increase in contrast to the as-grown sample (GNP-2a) for the $^5D_0$–^7F_J transition. The variation of lifetime constants on iron ions concentration in the starting materials can also be attributed to the influence of crystallinity. On increasing the iron content in the starting materials, the Gd_2O_3:Eu^{3+} products inevitably create more lattice defects, which act as quenching centers, even though there is no iron element in the final products. When an excited luminescent center (Eu^{3+}) is close to a trap, the excited energy is able to be nonradiatively transferred to the nearby traps. This leads the nonradiative transition rate from $^5D_0$ to increase, and the lifetime constants to decrease from the GNP-1a to the GNP-4a sample. The increase in luminescent lifetime constants in the Gd_2O_3:Eu^{3+}@SiO_2 sample could be attributed to the decrease in nonradiative transition rate due to surface modification [22]. In addition, the variation of refractive index in the composites will also lead to the change in radiative transition rate. The lifetime constants for the $^5D_1$–$^7F_1$ transitions of the Eu^{3+} ions in different samples are also listed in Table 1. The decay time constants also gradually decrease with increasing the iron concentration in the starting material on the whole, for the $^5D_1$–$^7F_1$ transitions.

4. Conclusions

A series of uniform, monodisperse Gd_2O_3: Eu^{3+} nanospheres ($<$100 nm) have been successfully synthesized via the DMF solvothermal synthesis procedure. Meanwhile, a facile and straightforward synthetic method to prepare bio-nanocomposites containing a luminescent core and a silica shell has been developed. The results demonstrate that coexistence of CTAB, PVP and iron chloride or acid is important for the formation of $Gd(OH)_3$:Eu^{3+} as well as Gd_2O_3:Eu^{3+} nanospheres in the DMF solvothermal solution. The increase in iron chloride in the starting material could increase the rate of aggregation to induce to the poor crystallinity of Gd_2O_3:Eu^{3+} nanocrystals. As a consequence, the luminescent intensity of $^5D_0$–^7F_J transitions gradually quenches, while the lifetime constant becomes short gradually. In the Gd_2O_3:Eu^{3+}@SiO_2 sample, the overall intensity of $^5D_0$–^7F_J decreases; however, the lifetime of $^5D_0$–^7F_J is prolonged. This work is significant for the synthesis of RE nanophosphors applied in the biomedical fields.

Table 1
A list of luminescent decay time constants of different samples.

Sample	$^5D_0$–$^7F_2$ λ_{em}=612 nm				$^5D_1$–$^7F_1$ λ_{em}=534 nm			
	I_1*	τ_1 (ms)	I_2*	τ_2 (ms)	I_1*	τ_1 (μs)	I_2*	τ_2(μs)
GNP-1a	0.567	0.22	0.422	0.91	0.573	15.6	0.424	42.9
GNP-2a	0.557	0.19	0.467	0.77	0.386	13.2	0.612	36.3
GNP-3a	0.600	0.19	0.408	0.73	0.660	16.7	0.348	45.2
GNP-4a	0.642	0.12	0.365	0.46	0.467	11.3	0.548	34.8
Gd_2O_3@SiO_2	0.516	0.18	0.433	1.06	0.331	9.3	0.663	32.9

Acknowledgments

The authors are thankful for the High-Tech Research and development Program of China (863) (Grant no. 2007AA03Z314) and the National Natural Science Foundation of China (Grant nos. 20971051, 50772042 and 10704073). We are very grateful to Prof. Jihong Yu for her helpful discussion and structural characterization. We are also grateful to Prof. Junqi Sun for his helpful discussion.

Appendix A. Supporting information

Supplementary data associated with this article can be found in the online version at doi:10.1016/j.jssc.2010.09.002.

References

[1] (a) Y. Sun., Y. Xia, Science 298 (2002) 2176–2179;
(b) Y. Yin, R.M. Rioux, C.K. Erdonmez, S. Hughes, G.A. Somorjai, A.P. Alivisatos, Science 304 (2004) 711–714.
[2] F. Shi, M.K. Tse, M.M. Pohl, A. Brückner, S.M. Zhang, M. Beller, Angew. Chem. Int. Ed. 46 (2007) 8866–8868.
[3] (a) X.M. Lu, H.Y. Tuan, J.Y. Chen, Z.Y. Li, B.A. Korgel, Y.N. Xia., J. Am. Chem. Soc. 129 (2007) 1733–1742;
(b) B. Liu, H.C. Zeng, J. Am. Chem. Soc. 126 (2004) 16744–16746;
(c) C.J. Jia, L.D. Sun, Z.G. Yan, L.P. You, F. Luo, X.D. Han, Y.C. Pang, Z. Zhang, C.H. Yan, Angew. Chem. Int. Ed. 44 (2005) 4328–4333.
[4] (a) H. Zeng, S.H. Sun, Adv. Funct. Mater. 18 (2008) 391–400;
(b) J.N. Park, K.J. An, Y. Hwang, J.G. Park, H.J. Noh, J.Y. Kim, J.H. Park, N.M. Hwang, T. Hyeon, Nature Mater. 3 (2004) 891–895.
[5] (a) Y.H. Deng, D.W. Qi, C.H. Deng, X.M. Zhang, D.Y. Zhao, J. Am. Chem. Soc. 130 (2008) 28–29;
(b) M. Yin, Y. Gu, I.L. Kuskovsky, T. Andelman, Y. Zhu, G.F. Neumark, S.J. O'Brien, J. Am. Chem. Soc. 126 (2004) 6206–6207.
[6] (a) X.H. Li, D.H. Zhang, J.S. Chen, J. Am. Chem. Soc. 128 (2006) 8382–8383;
(b) X. Wang, J. Zhuang, Q. Pen, Y.D. Li, Inorg. Chem. 45 (2006) 6661–6665.
[7] K.L. Ai, B.H. Zhang, L.H. Lu, Angew. Chem. Int. Ed. 48 (2009) 304–308.
[8] (a) R. Kumar, M. Nyk, T.Y. Ohulchanskyy, C.A. Flask, P.N. Prasad, Adv. Funct. Mater. 19 (2009) 853–859;
(b) C.C. Huang, W. Huang, C.H. Su, C.N. Feng, W.S. Kuoa, C.S. Yeh, Chem. Commun. (2009) 3360–3362.
[9] (a) Y.F. Xu, D.K. Ma, X.A. Chen, D.P. Yang, S.M. Huang, Langmuir 25 (2009) 7103–7108;
(b) G. Jia, H.P. You, M. Yang, L.H. Zhang, H.J. Zhang, J. Phys. Chem. C 113 (2009) 16638–16644.
[10] (a) G.F. Wang, Q. Peng, Y.D. Li, J. Am. Chem. Soc. 131 (2009) 14200–14201;
(b) C.X. Li, Z.Y. Hou, C.M. Zhang, P.P. Yang, G.G. Li, Z.H. Xu, Y. Fan, J. Lin, Chem. Mater. 21 (2009) 4598–4607.
[11] S.E. Skrabalak, B.J. Wiley, M. Kim, E.V. Formo, Y. Xia, Nano Lett. 8 (7) (2008) 2077–2081.
[12] F. Cao, W.D. Shi, L.J. Zhao, S.Y. Song, J.H. Yang, Y.Q. Lei, H.J. Zhang, J. Phys. Chem. C. 112 (2008) 17095–17101.
[13] J. Yang, C.K. Lin, Z.L. Wang, J. Lin, Inorg. Chem. 45 (2006) 8973–8979.
[14] (a) K. Binnemans, Chem. Rev. 109 (2009) 4283–4374;
(b) K.A. Abel, J.C. Boyer, F.C.J.M. Van Veggel, J. Am. Chem. Soc. 131 (2009) 14644–14645.
[15] (a) H. Schafer, P. Ptacek, H. Eickmeier, M. Haase, Adv. Funct. Mater. 19 (2009) 3091–3097;
(b) Y.P. Li, J.H. Zhang, X. Zhang, Y.S. Luo, X.G. Ren, H.F. Zhao, X.J. Wang, L.D. Sun, C.H. Yan, J. Phys. Chem. C. 113 (2009) 4413–4418.
[16] (a) V. Mahalingam, F. Vetrone, R. Naccache, A. Speghini, J.A. Capobianco, Adv. Mater. 21 (2009) 4025–4028;
(b) Z.X. Li, L.L. Li, H.P. Zhou, Q. Yuan, C. Chen, L.D. Sun, C.H. Yan, Chem. Commun. (2009) 6616–6618.
[17] (a) X.M. Liu, J.W. Zhao, Y.J. Sun, K. Song, Y. Yu, C. Du, X.G. Kong, H. Zhang, Chem. Commun. (2009) 6628–6630;
(b) G.H. Pan, H.W. Song, X. Bai, Z.X. Liu, H.Q. Yu, W.H. Di, S.W. Li, L.B. Fan, X.G. Ren, S.Z. Lu, Chem. Mater. 18 (2006) 4526–4532;
(c) A. Patra, C.S. Friend, R. Kapoor, P.N. Prasad, J. Phys. Chem. B. 106 (2002) 1909–1912.
[18] Z.H. Xu, C.X. Li, P.P. Yang, C.M. Zhang, S.S. Huang, Jun Lin, Cryst. Growth Des. 9 (2009) 4752–4758.
[19] (a) L.F. Hu, R.Z. Ma, T.C. Ozawa, T. Sasaki, Angew. Chem. Int. Ed. 48 (2009) 3846–3849;
(b) Y.P. Li, J.H. Zhang, X. Zhang, Y.S. Luo, S.Z. Lu, Z.D. Hao, X.J. Wang, J. Phys. Chem. C. 113 (2009) 17705–17710.
[20] (a) J. Yang, Z.W. Quan, D.Y. Kong, X.M. Liu, J. Lin, Cryst. Growth Des. 7 (2007) 730–735;
(b) H. Wang, C.K. Lin, X.M. Liu, J. Lin, M. Yu, Appl. Phys. Lett. 87 (2005) 181907;
(c) M. Yu, J. Lin, J.Y. Fang, Chem. Mater. 17 (2005) 1783–1791.
[21] G.H. Pan, H.W. Song, X. Bai, L.B. Fan, H.Q. Yu, Q.L. Dai, B. Dong, R.F. Qin, S.W. Li, S.Z. Lu, X.G. Ren, H.F. Zhao, J. Phys. Chem. C. 111 (2007) 12472–12477.
[22] X. Bai, H.W. Song, G.H. Pan, Z.X. Liu, S.Z. Lu, W.H. Di, X.G. Ren, Y.Q. Lei, Q.L. Dai, L.B. Fan, Appl. Phys. Lett. 88 (2006) 143104.
[23] M. Yada, M. Mihara, S. Mouri, M. Kuroki, T. Kijima, Adv. Mater. 14 (2002) 309–313.
[24] M.Z. Yao, A.G. Joly, W. Chen, J. Phys. Chem. C 114 (2010) 826–831.
[25] (a) X. Bai, H.W. Song, G.H. Pan, Y.Q. Lei, T. Wang, X.G. Ren, S.Z. Lu, B. Dong, Q.L. Dai, L.B. Fan, J. Phys. Chem. C 111 (2007) 13611–13617;
(b) F. Zhang, D.Y. Zhao, ACS Nano 3 (1) (2009) 159–164.
[26] A.W. Xu, Y.P. Fang, L.P. You, H.Q. Liu, J. Am. Chem. Soc. 125 (2003) 1494–1495.
[27] M. Buijs, A. Meyerink, G. Blasse, J. Lumin. 37 (1987) 9–20.
[28] H. Hu, M.X. Yu, F.Y. Li, Z.G. Chen, X. Gao, L.Q. Xiong, C.H. Huang, Chem. Mater. 20 (2008) 7003–7009.
[29] P. Li, Q. Peng, Y.D. Li, Adv. Mater. 21 (2009) 1945–1948.
[30] M. Nichkova, D. Dosev, S.J. Gee, B.D. Hammock, L.M. Kennedy, Anal. Chem. 77 (2005) 6864–6873.
[31] I.F. Li, C.H. Su, H.S. Sheu, H.C. Chiu, Y.W. Lo, W.T. Lin, J.H. Chen, C.S. Yeh, Adv. Funct. Mater. 18 (2008) 766–776.
[32] M.F. Zhang, S.J. Shi, J.X. Meng, X.Q. Wang, H. Fan, Y.C. Zhu, X.Y. Wang, Y.T. Qian, J. Phys. Chem. C 112 (2008) 2825–2830.
[33] K.X. Yao, H.C. Zeng, J. Phys. Chem. C 111 (2007) 13301–13308.
[34] (a) Z.B. Zhuang, X.T. Lu, Q. Peng, Y.D. Li, J. Am. Chem. Soc. 132 (2010) 1819–1821;
(b) H.Y. Xiao, P.N. Li, F.L. Jia, L.Z. Zhang, J. Phys. Chem. C 113 (2009) 21041–21304.
[35] S.D. Han, J.D. Kima, K.S. Myung, Y.H. Lee, H. Yang, K.C. Singh, Mater. Chem. Phys. 103 (2007) 89–94.